Anisotropic Hypersonic Phonon Propagation in Films of Aligned Ellipsoids

Peter J. Beltramo, Dirk Schneider, George Fytas, and Eric M. Furst

Anisotropic hypersonic phonon propagation in films of aligned ellipsoids

Peter J. Beltramo,[1] Dirk Schneider,[2] George Fytas,[2, 3, *] and Eric M. Furst[1, †]

[1]*Department of Chemical & Biomolecular Engineering,*
Center for Molecular and Engineering Thermodynamics,
University of Delaware, Newark, Delaware 19716, USA
[2]*Max Planck Institute for Polymer Research, Ackermannweg 10, 55128 Mainz, Germany*
[3]*Department of Materials Science, University of Crete and IESL-FORTH, 71110 Heraklion, Greece*

A material with anisotropic elastic mechanical properties and a direction-dependent hypersonic band gap is fabricated using AC electric field-directed convective self-assembly of colloidal ellipsoids. The frequency of the gap, which is detected in the direction perpendicular to particle alignment and entirely absent parallel to alignment, and the effective sound velocities can be tuned by the particle aspect ratio. We hypothesize that the band gap originates from the primary eigenmode peak, the m-splitted $(s,1,2)$ mode, of the particle resonating with the effective medium. These results reveal the potential for powerful control of the hypersonic phononic band diagram by combining anisotropic particles and self-assembly.

Manipulation of the elastic energy propagation in materials is possible for frequencies ranging from audible $(20-10^4$ Hz) [1, 2] to hypersonic $(10^8-10^{11}$ Hz) [3–7] and has applications in phonon tunneling [8] and the transformation of wave propagation by deformation [9]. Because hypersonic waves are thermally activated and act as the main heat carrier in dielectrics, controlling phonon transport provides a means to engineer advanced heat management systems, such as thermal diodes in nanoelectronic materials or thermoelectrics for energy conversion [10].

Control over phonon propagation requires a material's mechanical properties to be tailored on the nanometer to micrometer scale. One route to achieving such mesoscale structures is by the self-assembly of small particles. The expanding library of uniform colloidal and nanoparticle building blocks with sophisticated shapes and interactions allows for the fabrication of complex structured, functional materials [11–13]. Previous work has examined phonon propagation in colloidal crystals from spherical building blocks [3, 4, 6, 14, 15]. Such structures exhibit a Bragg-type bandgap with a frequency and spectral width that can be tuned by the sphere diameter and infiltrating material [3]. Bandgaps at lower frequencies, termed hybridization gaps, have also been reported [4, 15, 16], and result from the level repulsion between the acoustic branch and a localized vibrational modes of the particle. Hybridization gaps persist even with the loss of structural order. For nanoparticles, bandgaps occur at gigahertz (GHz) frequencies and are easily measured by Brillouin light scattering (BLS). Previous BLS studies have characterized the eigenmode spectra of spheres [17–20] and their resulting phononic band diagram [3, 21, 22].

Until only recently [23, 24], the vibrational spectra of particles with more complex shapes had not been characterized, and the phononic band diagram of ordered arrays of anisotropic particles remains unstudied. In this Letter, we present the hypersonic phonon band diagram of aligned films of ellipsoids. We report anisotropy in the mechanical properties of the film and a unique

anisotropic band gap: one that is present in the direction perpendicular but not parallel to particle alignment. This result demonstrates that self-assembled colloidal metamaterials can be formed from anisotropic particles and provides for a new means to control the flow of acoustic and thermal energy in materials.

Nano-ellipsoids with three aspect ratios ($a/b = 2.12$, 3.52 and 3.99) are fabricated by mechanical stretching of 400 nm diameter carboxylate modified PS spheres (cat. #C37238, Invitrogen). The stretching procedure is described in detail elsewhere [25, 26]. The size of the ellipsoids is characterized by scanning electron microscopy (SEM) and the stretched axis length a is 690 ± 42 nm, 986 ± 15 nm, and 1078 ± 93 nm for the 2.12, 3.52 and 3.99 aspect ratio particles, respectively. The ellipsoids are suspended in 0.1 mM KCl and are concentrated to a volume fraction $\phi \approx 0.15$ before being introduced to the AC electric field assembly cell.

We assemble particles into orientationally ordered thin films by AC electric field-directed convective assembly [27, 28]. The assembly cell consists of coplanar gold electrodes on a glass slide with a $1.5-2$ mm electrode gap (Fig. 1a) [29]. The cell is placed on a temperature controlled stage at 22°C before loading $3-5 \mu$L of suspension by capillary forces at the open ends. An AC electric field (75 kHz, $500-700$ $V_{\rm rms}/$cm) is applied. The edges of the cell are left open, allowing the particles to align in suspension as a result of the applied field and advect towards the drying front at the edge of the cell to form an orientationally ordered thin film (Fig. 1a). SEM images show the orientational order persists throughout the ∼20 μm film thickness (Fig. 1b). Analysis of top-view SEM images of films fabricated with all three aspect ratios show that greater than 90% of the particles are aligned within ±30° of the electric field direction in every case (see SI). Field-aligning anisotropic particles in a more dilute suspension before concentrating the particles with convective deposition avoids jamming. This successful assembly path has also been used to crystallize slightly anisotropic
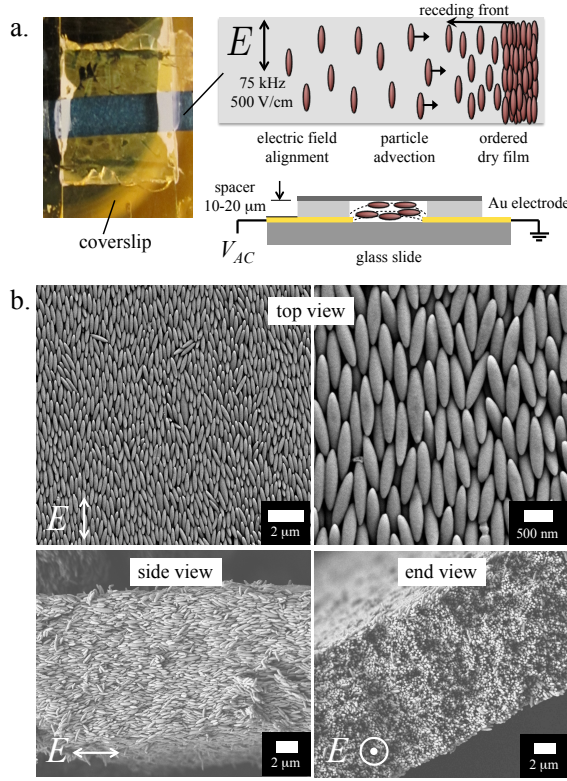
FIG. 1. (a) Schematic of the directed assembly process (not to scale). (b) SEM images of the top, side and end view of the resulting aligned film for $a/b = 3.99$.

magnetic ellipsoids [30], align titania ellipsoids [27] and crystallize PS dicolloids [28]. After drying, the top coverslip is removed, keeping the film intact and allowing infiltration with poly(dimethylsiloxane) (PDMS, $M_w = 770$ Da) for BLS measurements. The sample is rotated to measure thermal phonon propagation either parallel ($q_\parallel$) or perpendicular ($q_\perp$) to the particle alignment.

High-resolution BLS measurements of the films are performed using a six-pass tandem Fabry-Perot interferometer in conjunction with a $\lambda = 532$ nm Nd/YAG laser mounted on a goniometer, allowing for q-dependent experiments [4, 31]. Thermally excited phonons along $\mathbf{q} = \mathbf{k}_s - \mathbf{k}_i$ cause inelastic scattering of the incident laser (photon). Here $\mathbf{k}_i$ and $\mathbf{k}_s$ refer to the incident and scattered photon wavevector, respectively. The scattering vector $\mathbf{q}$ is equal to the phonon wavevector. Dispersion relations are obtained by recording the phonon frequencies as a function of scattering wavevector $\mathbf{q}$. The BLS spectrum consists of doublets centered around the elastic frequency with $f = \pm c_L q / 2\pi$, where c_L is the longitudinal sound velocity for homogeneous (over the probed length scale) films. Spectra are obtained over a q-range of $0.0041 - 0.0205$ nm^{-1}. The free spectral range varies between 6, 7.5 and 10 GHz depending on the scattering angle to achieve optimal resolution of the phonon peak.

For turbid (uninfiltrated) samples, multiple scattering causes $\mathbf{q}$ to be ill-defined, however, $\mathbf{q}$-independent resonance modes of the individual colloidal ellipsoids are still measured [24]. The particle vibration spectra of opaque (prior to infiltration with PDMS) aligned particle films is checked and is consistent with isotropic particle films (see SI). Measurements of infiltrated, index matched films allow access to the q-dependent acoustic modes along the desired propagation direction.

The BLS spectra of the $a/b = 2.12$ and 3.52 aspect ratio aligned films at selected q values above, near, and below the hybridization gap (HG, discussed later) are shown in Fig. 2a (see SI for $a/b = 3.99$). For clarity, only the anti-Stokes contributions of the symmetric BLS spectra are included. At low $q = 0.0081$ nm^{-1}, the material appears homogeneous and a single Lorentzian peak is seen in both directions. The peak occurs at a higher frequency in the direction parallel to the long axis of the particle. As q increases, the peak width increases and two peaks appear in the spectra at the intermediate q-value. This splitting of a single peak as q increases is the consequence of a band gap in the material [3, 21]. At high q, the anisotropy in the spectra as a result of propagation direction is still clear, with peaks occurring at a higher frequency for the $q_\parallel$ than the $q_\perp$ direction at a given scattering angle.

The noteworthy features of Fig. 2a are apparent in the corresponding phonon dispersion plots, Fig. 2b-d. First, the frequency of the acoustic peaks $f(q)$ varies with propagation direction over the entire range of q. Parallel to the particle alignment, $f(q)$ is linear, representing an effective medium longitudinal sound velocity $c_L = 1750 \pm 80$, 1900 ± 50 and 1850 ± 50 ms^{-1} for the $a/b = 2.12$, 3.52 and 3.99 ellipsoid aspect ratios, respectively (Fig. 2c). These values are significantly higher than that found for the seed spheres infiltrated by the same PDMS liquid, in which $c_L = 1460 \pm 10$ ms^{-1}. At low-q in the direction perpendicular to the particle alignment (Fig. 2d), $f(q)$ is also linear, however, the effective longitudinal sound velocity in all three films is close to that of the infiltrated crystal of the seed spheres.

Strikingly, the phonon dispersion relation demonstrates that structures of aligned ellipsoids exhibit anisotropic acoustic properties. Furthermore, the degree of stretching dictates the effective sound velocity *in the parallel direction only*, while remaining constant (and similar to the seed spheres) in the perpendicular direction (Fig. 3, top).

Two possible mechanisms could explain the anisotropic longitudinal sound velocity in the ellipsoid films. One possibility is that increased PS/PDMS grain boundaries in the perpendicular versus parallel direction could delay phonon propagation in that direction, e.g. via strong phonon scattering. While the volume fraction is of course constant along either direction in the film, the anisotropic average center-center particle spacing could contribute
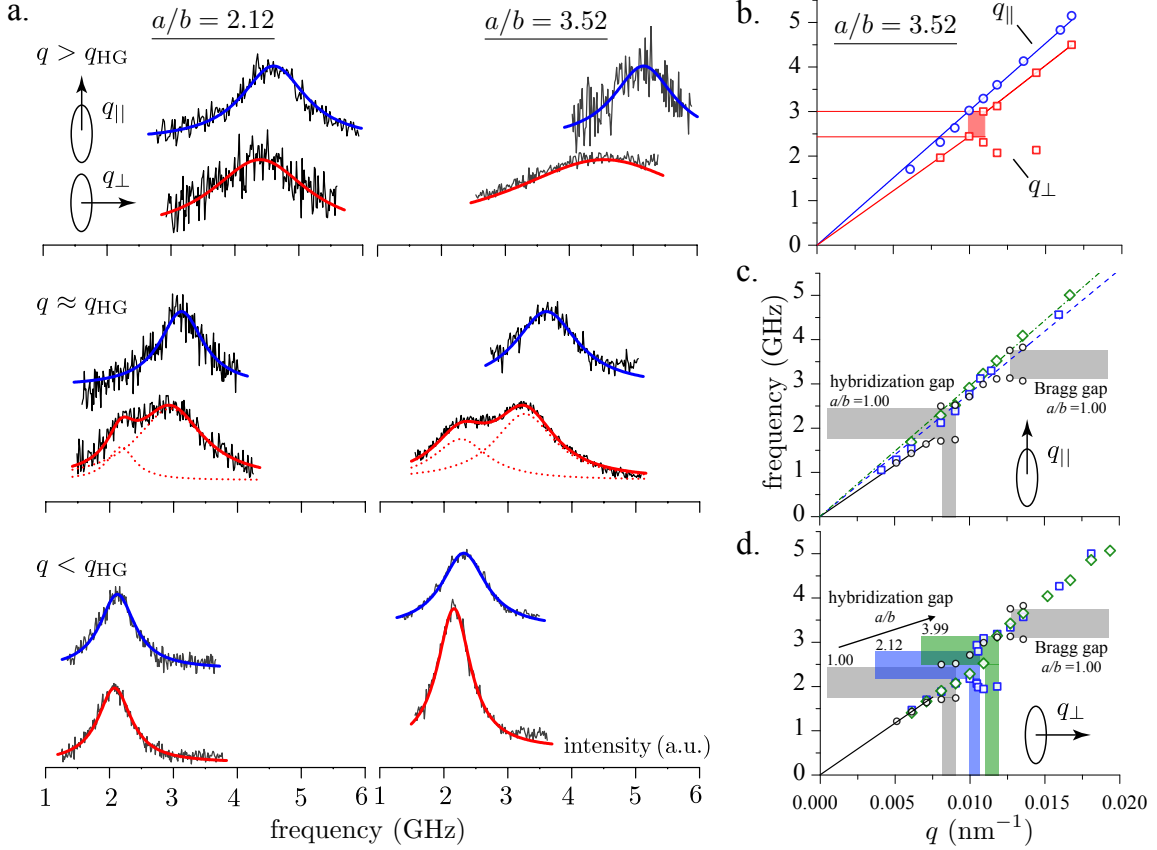
FIG. 2. (a) Selected BLS spectra of the infiltrated aligned films with aspect ratio $a/b = 2.12$ and 3.52 at scattering wavevector q values below (0.0081 nm^{-1}), near (0.0106 nm^{-1} for 2.12; 0.0118 nm^{-1} for 3.52) and above (0.0160 nm^{-1} for 2.12; 0.0167 nm^{-1} for 3.52) the value q_{HG} where the anisotropic hybridization gap (HG) opens. The anti-Stokes BLS spectra for propagation along ($q_{\parallel}$, blue) and normal ($q_{\perp}$, red) to the long axis are represented by either one or the sum of two Lorentzian curves (dotted lines). (b) Phononic band diagram for the $a/b = 3.52$ aligned film in both propagation directions. A band gap (shaded region) is only observed in the $q_{\perp}$ direction (indicated by the horizontal red lines). (c) Phononic band diagram in the $q_{\parallel}$ propagation direction for $a/b = 2.12$ (blue squares) and 3.99 (green diamonds) with seed spheres (black circles) as a reference. The lines fit the effective longitudinal sound velocity. (d) Same as (c) but for the $q_{\perp}$ propagation direction. The shaded regions indicate the frequency and scattering wavevector of the HG. The assembled spheres exhibit a Bragg-type band gap at high frequencies in addition to the HG irrespective of the direction.

to the anisotropic sound velocity in a way analogous to that of acoustic metamaterials[32]. Another explanation is that the unidirectional stretching procedure may cause different elastic moduli of PS inside the particle, depending on direction. This may help explain results from our previous study on the single ellipsoid eigenmode spectra that showed decreased particle density (increased elastic moduli) with asphericity was needed to model the single particle vibration spectra [24]. The effective sound velocity is also a function of the particle packing fraction. All films are fabricated by the same method, and estimates of the packing fraction from SEM images leads to a consistent $\phi \approx 0.7$ across all films. This packing fraction is lower than the maximum theoretical packing of a simple monoclinic phase, $\phi = 0.77$, for ellipsoids due to the lack of translational particle order in the sample films[33, 34].

Based on the similar dissipation, evident by the width of the BLS spectra in the lower panel of Fig. 2a, the second mechanism seems to be more probable. However, the absence of an exact effective medium theory for the density and moduli of soft materials[32, 35] renders a quantitative assignment of the two elastic moduli of PS inside the ellipsoid particle ambiguous.

The second important feature of the BLS measurements is the presence of a propagation direction-dependent bandgap in the films. Centered at a frequency (q value) of 2.49 GHz (0.0103 nm^{-1}), 2.72 GHz (0.0104 nm^{-1}) and 2.84 GHz (0.0114 nm^{-1}) for the 2.12, 3.52 and 3.99 aspect ratio particles, respectively, the peak in each spectrum splits and the slope of the dispersion, $f(q)$, in the *perpendicular* direction changes (Fig. 2d). The peak splitting is clearly seen in the spectra of $a/b = 2.12$ and
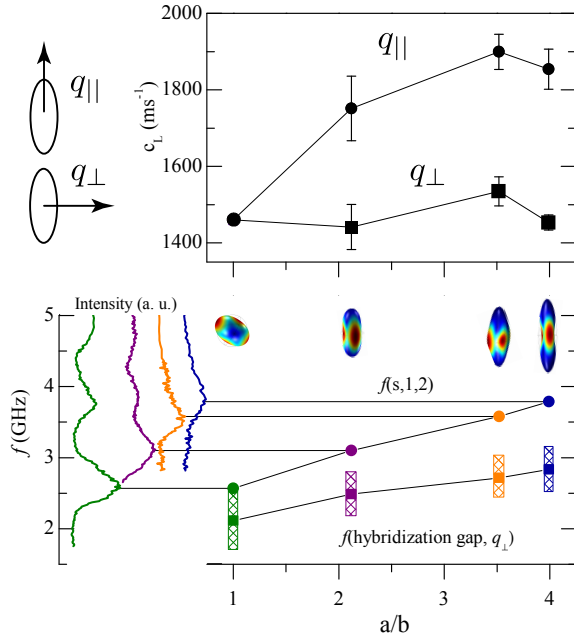
FIG. 3. (top) The effective sound velocity as a function of particle aspect ratio and thermal phonon propagation direction. (bottom) q-independent eigenmode spectra of seed spheres and ellipsoids (left panel) and frequency dependence of the m-splitted $(s,1,2)$ peak and the hybridization gap in the $q_\perp$ direction. Inset images are FEM calculations for the vibrational deformation of the primary eigenmode peak.

of the particle is lost [24]; (s, n, l, m) label the radial (n) and angular (l, m) particle vibrations. However, the $m = 0$ mode shifts to lower frequencies while the $m = 2$ mode moves to higher frequencies. It is this latter mode that gives the strongest peak in the BLS eigenmode spectrum and has the same frequency dependence across different aspect ratios as the observed gap (Fig. 3, bottom). Due to differences in the mechanical properties between PDMS and air, one would not expect the frequencies to be the same [21], but the similar dependence implies that the origin of the gap is hybridization of the $m = 2$ spheroidal vibration $(s,1,2)$ mode of the particle with the acoustic branch of the effective medium. The collective particle alignment results in a tangible difference in the direction dependent bulk phonon properties.

Finite element method (FEM) calculations of the displacement of this mode reveal it is essentially a "pinching" of the short axis (b) of the ellipsoid. Since the perpendicular direction is measuring propagation across this short axis, we suspect the anti-crossing interaction of this vibrational state with the propagating acoustic wave should occur in only this direction [37]. As a result, the HG appears only in the $q_\perp$ direction. FEM calculations of the $m = 0$ $(s,1,2)$ mode reveal that this deformation is a stretching of the particle along the long axis (a). This mode exhibits weaker intensity and appears at lower frequencies due to the longer length scale (long axis of the particle, lower q). Therefore, observing a HG in the $q_\parallel$ direction is unlikely given the size of the particles $(a > b$, lower q) and the BLS instrumental resolution.

The need for orientational order to produce a HG in the ellipsoid films may at first appear to contrast the behavior of the HG in infiltrated spheres, where the gap persists upon the loss of structural order in the sample [21]. However, with anisotropic particles, orientational order is a prerequisite to define the probed direction through the wave vector q relative to the particle and isolate specific vibrational states to interact with the propagating acoustic wave.

Lastly, since the particles have good orientational order, but are not arranged on a periodic crystal lattice, a Bragg gap is not observed at higher q in the ellipsoid films. Refining self-assembly techniques to achieve such robust control over translational order in addition to the orientational order shown here may lead to new functional materials. Possible approaches towards this end include tuning interparticle interactions by either orthogonal directing fields, or chemically via particle patchiness. Perhaps, the *simultaneous* realization of anisotropic Bragg gaps (tunable by lattice vector, or the dimensions of the colloidal building blocks) and a unidirectional hybridization gap (tunable by aspect ratio and packing fraction) could be achieved.

In conclusion, we have shown that AC field-directed convective self-assembly can be used to fabricate a material with complex acoustic properties. Due to shape

3.52 (Fig. 2a) and the change in slope is pronounced in the 3.99 aspect ratio film despite the absence of peak splitting. The band gap is further confirmed in the 3.99 aspect ratio sample by blocking of the acoustic phonons from an excess PDMS layer on top of the infiltrated film (see SI).

This gap is absent in the parallel direction, where $f(q)$ is linear and a single acoustic phonon with a constant speed of sound is observed over the entire measured q-range (Fig. 2c). While the gap is shifted to higher $q_\perp$ and hence frequency with decreasing b, the gap width remains virtually constant (lower panel of Fig. 3). Since the latter depends on the elastic impedance contrast, a robust gap width implies a constant sound velocity in the perpendicular direction in agreement with the effective sound velocity results in Fig. 3. We have deliberately chosen to measure in the two high symmetry directions, $q_\parallel$ and $q_\perp$. As the propagation direction shifts from the perpendicular to parallel direction, we suspect the band gap will decrease in bandwidth as the deviation from $q_\perp$ increases, similar to that observed for Bragg gaps in one dimensional multilayer stacks [36].

Our previous study of the eigenmode spectra of the same particles revealed the spheroidal $(s,1,2)$ vibration mode of the seed spheres splits into multiple $(2l + 1)$ modes due to lifted mode degeneracy as the symmetry

anisotropy in the ellipsoidal building blocks, acoustic phonons propagate with different velocities parallel and perpendicular to their orientation, a phenomenon that has been observed previously for only macroscale acoustic metamaterials. An anisotropic band gap was found. The location of the band gap and its frequency dependence with the particle aspect ratio indicates that this is a hybridization type gap. Realizing such a gap was unexpected considering the complexity of the ellipsoid eigenmodes, namely the selection rules, parity of the modes and lifting the m-degeneracy. Hence, it appears that particle alignment is an additional requirement for hybridization gaps in materials made from anisotropic building blocks. Soft matter colloids provide a unique material to study the phonon-matter interactions in self-assembled materials. As self-assembly techniques are applied to additional anisotropic building blocks, the creation of increasingly complex structures will lead to further control over the phononic band structure and thus the propagation of elastic waves (sound) and heat in nanostructures.

---

* fytas@mpip-mainz.mpg.de

† furst@udel.edu

[1] R. Martínez-Sala, J. Sancho, J. V. Sánchez, V. Gómez, J. Llinares, and F. Meseguer, nature **378**, 241 (1995).

[2] Z. Liu, X. Zhang, Y. Mao, Y. Y. Zhu, Z. Yang, C. T. Chan, and P. Sheng, Science **289**, 1734 (2000).

[3] W. Cheng, J. Wang, U. Jonas, G. Fytas, and N. Stefanou, Nature Materials **5**, 830 (2006).

[4] T. Still, W. Cheng, M. Retsch, U. Jonas, and G. Fytas, J Phys-Condens Mat **20**, 404203 (2008).

[5] T. Gorishnyy, J.-H. Jang, C. Koh, and E. L. Thomas, Appl. Phys. Lett. **91**, 121915 (2007).

[6] A. Akimov, Y. Tanaka, A. Pevtsov, S. Kaplan, V. Golubev, S. Tamura, D. Yakovlev, and M. Bayer, Phys. Rev. Lett. **101**, 033902 (2008).

[7] G. Zhu, N. Z. Swinteck, S. Wu, J. S. Zhang, H. Pan, J. D. Bass, P. A. Deymier, D. Banerjee, and K. Yano, Phys. Rev. B **88**, 144307 (2013).

[8] S. Yang, J. Page, Z. Liu, M. Cowan, C. Chan, and P. Sheng, Phys. Rev. Lett. **88**, 104301 (2002).

[9] S. Rudykh and M. C. Boyce, Phys. Rev. Lett. **112**, 034301 (2014).

[10] M. Maldovan, Nature **503**, 209 (2013).

[11] S. C. Glotzer and M. J. Solomon, Nature Materials **6**, 557 (2007).

[12] M. Grzelczak, J. Vermant, E. M. Furst, and L. M. Liz-Marzan, ACS Nano **4**, 3591 (2010).

[13] S. Sacanna and D. J. Pine, Curr. Opin. Colloid Interface Sci. **16**, 96 (2011).

[14] M. Mattarelli, M. Secchi, and M. Montagna, J. Chem. Phys. **139**, 174710 (2013).

[15] N. Boechler, J. K. Eliason, A. Kumar, A. A. Maznev, K. A. Nelson, and N. Fang, Phys. Rev. Lett. **111**, 036103 (2013).

[16] M. L. Cowan, J. H. Page, and P. Sheng, Phys. Rev. B **84**, 094305 (2011).

[17] M. Kuok, H. Lim, S. Ng, N. Liu, and Z. Wang, Phys. Rev. Lett. **90**, 255502 (2003).

[18] M. Pelton, J. E. Sader, J. Burgin, M. Liu, P. Guyot-Sionnest, and D. Gosztola, Nat Nano **4**, 492 (2009).

[19] T. Still, M. Mattarelli, D. Kiefer, G. Fytas, and M. Montagna, J Phys Chem Lett **1**, 2440 (2010).

[20] M. Mattarelli, M. Montagna, T. Still, D. Schneider, and G. Fytas, Soft Matter **8**, 4235 (2012).

[21] T. Still, W. Cheng, M. Retsch, R. Sainidou, J. Wang, U. Jonas, N. Stefanou, and G. Fytas, Phys. Rev. Lett. **100**, 194301 (2008).

[22] T. Still, G. Gantzounis, D. Kiefer, G. Hellmann, R. Sainidou, G. Fytas, and N. Stefanou, Phys. Rev. Lett. **106**, 175505 (2011).

[23] J. Y. Sun, Z. K. Wang, H. S. Lim, V. L. Zhang, S. C. Ng, M. H. Kuok, W. Zhang, S. Firdoz, and X. M. Lu, J. Colloid Interface Sci. **152**, 501 (2012).

[24] D. Schneider, P. J. Beltramo, M. Mattarelli, P. Pfleiderer, J. Vermant, D. Crespy, M. Montagna, E. M. Furst, and G. Fytas, Soft Matter **9**, 9129 (2013).

[25] C. Ho, A. Keller, J. A. Odell, and R. H. Ottewill, **271**, 469 (1993).

[26] K. M. Keville, E. I. Franses, and J. M. Caruthers, J. Colloid Interface Sci. **144**, 103 (1991).

[27] M. Mittal and E. M. Furst, Adv. Funct. Mater. **19**, 3271 (2009).

[28] J. D. Forster, J.-G. Park, M. Mittal, H. Noh, C. F. Schreck, C. S. O'Hern, H. Cao, E. M. Furst, and E. R. Dufresne, ACS Nano **5**, 6695 (2011).

[29] S. Lumsdon, E. W. Kaler, and O. D. Velev, Langmuir **20**, 2108 (2004).

[30] T. Ding, K. Song, K. Clays, and C.-H. Tung, Adv Mater **21**, 1936 (2009).

[31] R. S. Penciu, H. Kriegs, G. Petekidis, G. Fytas, and E. N. Economou, J. Chem. Phys. **118**, 5224 (2003).

[32] D. Torrent and J. Sánchez-Dehesa, New J. Phys. **10**, 023004 (2008).

[33] A. Donev, F. H. Stillinger, P. M. Chaikin, and S. Torquato, Phys. Rev. Lett. **92**, 255506 (2004).

[34] P. Pfleiderer and T. Schilling, Phys Rev E **75**, 020402 (2007).

[35] J. Mei, Z. Liu, W. Wen, and P. Sheng, Phys. Rev. Lett. **96**, 024301 (2006).

[36] D. Schneider, F. Liaqat, E. H. El Boudouti, Y. El Hassouani, B. Djafari-Rouhani, W. Tremel, H.-J. Butt, and G. Fytas, Nano Lett **12**, 3101 (2012).

[37] G. Gantzounis, N. Papanikolaou, and N. Stefanou, Phys. Rev. B **83**, 214301 (2011).